NPL REPORT IR 1

Gel dosimetry for direct measurement of dose distributions: Progress report

J A D PEARCE and
D C CROSSLEY

NOT RESTRICTED

OCTOBER 2007

Gel dosimetry for direct measurement of dose distributions: Progress report

J A D Pearce and D C Crossley
Division for the Quality of Life

ABSTRACT

Gel dosimeters are based on chemical dosimeters in which radiation induced chemical reactions occur. The addition of gelling agents such as gelatin to certain chemical dosimeters can enable these chemical reactions to be stabilised spatially, which enables the 3 dimensional distribution of the dose within the volume of the dosimeter to be determined. A gel dosimeter based on the Fricke dosimeter has been investigated. A series of measurements to characterise the Fricke gel have been summarised in this report. Progress in the development of an optical computed tomography system and associated reconstruction software is also reviewed.

ISSN 1754-2952

National Physical Laboratory
Hampton Road, Teddington, Middlesex, TW11 0LW

Approved on behalf of the Managing Director, NPL
by Dr Martyn Sené, Director, Division for the Quality of Life

CONTENTS

1 INTRODUCTION 1
2 GEL DOSIMETRY OVERVIEW 2
2.1 Gel formations 2
2.1.1 Fricke gels 2
2.1.2 Polymer gels 3
2.1.3 PRESAGE 4
2.2 Readout methods 4
2.2.1 Magnetic resonance imaging 4
2.2.2 Optical computer tomography 5
3 METHOD 5
3.1 Preparation of gel 5
3.2 Irradiations 5
3.3 Spectrophotometry of the FSX gel 6
3.4 Refractive index of FSX gel 6
4 OPTICS 7
4.1 Set-up 7
4.2 Matching medium 8
4.3 Test phantom 8
5 SOFTWARE 8
6 RESULTS 8
6.1 Cuvette irradiations 8
6.2 Gel response at lower temperatures 12
6.3 Reproducibility of unirradiated gel 13
6.4 Reproducibility of radiation response 14
6.5 Cuvettes of gel held in normal light and darkness. 15
6.6 Plugs of gel from the circular holder 16
7 DISCUSSION 16
7.1 Cuvette irradiations 16
7.2 Gel response at low temperatures 17
7.3 Reproducibility 17
7.4 Samples of gel from the circular holder 17
8 CONCLUSION 18
9 REFERENCES 19
10 APPENDIX A: Procedure for gel preparation 22
11 APPENDIX B: Tomography program 24
12 APPENDIX C: Reconstruction program 26

FIGURES

Figure 1. A typical optical CT layout 7
Figure 2. Absorbance as a function of wavelength for a range of doses at 0 and 10 hours after irradiation 9
Figure 3. Absorbance as a function of dose at 0 and 10 hours after irradiation: 543nm 10
Figure 4. Absorbance as a function of dose at 0 and 10 hours after irradiation: 586nm 10
Figure 5. Change in measured dose with time for doses between 0 and 20 Gy: 543nm 11
Figure 6. Change in measured dose with time for doses between 0 and 20 Gy: 586nm 11
Figure 7. Change in measured dose with time for doses between 0 and 22 Gy at 586 nm for gel measured at 10 ± 2 °C. 12
Figure 8. Increase in measured dose over a period of 10 hours after irradiation for samples stored at 10 ºC and 22 ºC. 13
Doses in each case were ~20 Gy, but were not equal. Data shown is for measurements made at 586 nm. 13
Figure 9. Change in absorbance as a function of dose for different batches: 543nm 15
Figure 10. Change in absorbance as a function of dose for different batches: 586nm 15
Figure A1. Stirring the heated gelatin/H_2SO_4 solution 23
Figure A2. The gel holder 23
Figure B1. The gelOCT window showing the image recorded by the camera 24
Figure B2. The stepper motor set-up 24
Figure B3. The tomography control window 25

TABLES

Table 1. Comparison of increase in measured dose over a period 0.2 hours for samples stored at 10 and 22 °C. 13
Table 2. Effective background dose of unirradiated gel samples: 543 nm 14
Table 3. Effective background dose of unirradiated gel samples: 586 nm 14
Table 4. Absorbance of the plugs of gel 16

1 INTRODUCTION

Radiotherapy is one of the main treatment modalities for cancer. The aim of radiotherapy is to deliver a prescribed dose of radiation to a tumour site while minimising the damage to normal tissue. The effectiveness of radiotherapy can be improved by conforming radiation dose distributions delivered to the shape of the tumour volume. Advances in the determination of the location and extent of a tumour have been made possible through medical imaging developments such as computed tomography (CT) and magnetic resonance imaging (MRI).

Recent progression in the field with treatments such as intensity modulated radiation therapy (IMRT) or brachytherapy have placed demands on existing methods of dosimetry. IMRT combined with the use of multi-leaf collimators can deliver radiation through many beams with different shapes to establish a dose distribution that conforms tightly to the planned target volume and limits radiation to critical organs. High dose rate (HDR) brachytherapy involves the insertion of a radioactive source into a tumour volume directly; this source may be stepped back with different dwell times to build a dose profile within the volume.

The success of radiotherapy in curing cancer is dependent on accurate determination of absorbed dose to water. For example, optimal treatment of some head and neck tumours requires that the dose delivered should be within only a few percent of that prescribed. With advances in treatment delivery and patient immobilisation techniques, greater tumour control can now be achieved, however more complex treatments may mean than any error in dose delivery can result in more serious complications. Accurate radiation dosimetry is essential to improve patient survival rates.

The aim of radiation dosimetry is to determine absorbed dose to water with very high accuracy and precision. For the more complex treatments outlined previously, a dosimeter must be integrating to accommodate the time varying dose delivered and have high spatial resolution to confirm dose distributions in areas that have steep dose gradients such as those delivered in HDR brachytherapy. It should allow 3 dimensional volumetric dosimetry and must have a high accuracy and ideally be tissue equivalent. It should be independent of direction and insensitive to photon energy spectrum and dose rate (Mather 2003). There are a number of dosimeters currently used to determine radiation dose in radiotherapy treatments. These include ionisation chambers, radiographic film, diode detectors, thermoluminescent detectors (TLDs) and calorimeters. Detailed descriptions of these dosimeters can be found in standard texts (Attix 1986, Johns and Cunningham 1983). However current dosimeters, such as ionisation chambers or radiographic film are only 1 and 2 dimensional dosimeters and so are limited in their ability to integrate dose over a 3 dimensional volume. As a result, gel dosimeters capable of measuring a dose distribution in 3 dimensions are being developed. The two main evaluation techniques for gel dosimetry are those of magnetic resonance imaging (MRI) and optical computed tomography (CT).

2 GEL DOSIMETRY OVERVIEW

2.1 Gel formations

Gel dosimetry is based on chemical reactions caused by the action of ionising radiation. The addition of gelling agents such as gelatin to certain chemical dosimeters can enable these chemical reactions to be stabilised spatially enabling the 3 dimensional distribution of the dose within the volume of the dosimeter to be determined. This was first suggested in the 1950s when colour changes produced by ionising radiation were observed in gels containing dyes (Venning 2006). Currently there are two main types of gels, ferrous sulphate or Fricke gels, and polymer gels. This work investigated Fricke gels, however there is a brief overview of polymer gels.

2.1.1 Fricke gels

The method under development at the NPL to determine dose distribution is a Fricke gel dosimeter, based on the classic 'Fricke' dosimeter (Fricke and Hart 1966). This system relies on the oxidation of ferrous ions in an aerated, acidic ferrous sulphate solution. The action of ionising radiation on the solution causes water decomposition to occur, and the hydrogen atoms that are produced react with oxygen to produce the hydroperoxyl radical.

$$H^{\bullet} + O_2 \rightarrow HO_2^{\bullet} \tag{1}$$

A series of reactions then completes the conversion of ferrous (Fe^{2+}) ions to ferric (Fe^{3+}) ions.

$$\begin{aligned} &Fe^{2+} + OH^{\bullet} \rightarrow Fe^{3+} + OH^{-} \\ &Fe^{2+} + HO_2^{\bullet} \rightarrow Fe^{3+} + HO_2^{-} \\ &HO_2^{-} + H_3O^{+} \rightarrow H_2O_2 + H_2O \\ &Fe^{2+} + H_2O_2 \rightarrow Fe^{3+} + OH^{\bullet} + OH^{-} \end{aligned} \tag{2}$$

The change in ferric ion concentration has been shown to be proportional to absorbed dose until depletion of either oxygen or ferrous ions causes saturation. The change in ferric ion concentration can be measured spectrophotometrically. In regular Fricke dosimetry, the absorption peak of ferric ions at 304 nm is utilised, the absorption of ferrous ions at this wavelength being negligible. The relation between change in ferric ion concentration and absorbed dose is given in equation (3).

$$\Delta[Fe^{3+}] = D \cdot G(Fe^{3+}) \cdot \rho \tag{3}$$

Where $\Delta[Fe^{3+}]$ is the change in ferric ion concentration in mol dm^{-3}, D is the dose in Gy, $G(Fe^{3+})$ is the radiation chemical yield of Fe^{3+} in mol J^{-1} and ρ is the density in kg dm^{-3}.

The radiation chemical yield of ferric ions, G, has historically been expressed in terms of the number of ferric ions liberated per 100 eV of absorbed energy. In regular Fricke dosimetry the ferric ion chemical yield is 1.61 μmol J^{-1} (15.5 Fe^{3+}/100eV) for Co-60 radiation (Fricke and Hart 1966). However in a Fricke gel system this value is increased

due to the addition of chemical pathways for the conversion of Fe^{2+} provided by the organic gel macromolecules (Schreiner L J 2004).

The standard Fricke gel system can be modified to produce a system in which radiation-induced colour changes occur in the visible spectrum, thus making it suitable for optical scanning. A commonly added chemical is the chelating agent xylenol orange (XO), which forms a coloured complex with ferric ions (Appleby and Leghrouz 1990). There are several advantages to using xylenol orange in this system. The Fe^{3+}-XO complex absorbs most strongly in the green spectral region and so the radiation exposure to the gel is visibly evident (Tarte *et al* 1997). The molar absorption coefficient of the complex in the green spectral region is about seven times greater than the coefficient of the ferric ion alone in UV at 304 nm, resulting in greater sensitivity.

There have been a number of limitations found with Fricke gel dosimetry. It is limited by continual post irradiation diffusion of ions in the dosimeter, resulting in blurring of dose distributions and loss of spatial resolution (Schultz *et al* 1990). Attempts to reduce this included using a different gelling agent, or adding a chelating agent to the gel. A chelating agent forms two or more coordinate bonds with a central ferrous or ferric ion and so the Fe^{3+}-XO complex will diffuse more slowly than the unattached ferric ion. This enables greater time to measure the radiation distribution before the ferric ions are spatially dispersed, (Rae *et al* 1996).

However, there are a number of advantages to Fricke gels. They are easy to prepare without requiring any special facilities, they are tissue equivalent over a very large photon energy range and are able to be read very soon after irradiation, (Schreiner 2004).

2.1.2 Polymer gels

Polymer gels have been suggested as an alternative to Fricke gels without the diffusion problem. Polymer gel dosimeters consist of a hydrogel in which monomers are dissolved. Upon irradiation, a radiation induced polymerisation of the monomers occurs. The degree of polymerisation is dose dependent. These gels are more stable than Fricke gels because the polymer chains formed after irradiation are too large to diffuse significantly through the gel matrix. Advantages of polymer gel dosimeters include energy independence over a large photon energy range, being able to integrate dose, tissue equivalence and the ability to record dose distributions in 3 dimensions, (De Deene 2004a).

There are several different types of polymer gel, discussed briefly here. These are most commonly readout using MRI, although optical readout is possible.

The BANG® gel consists of N,N'-methylene-bis-acrylamide monomers (bis) (3%), acrylamide (3%), nitrogen and gelatin (5%) (Maryanski *et al* 1994). This gel is now commercially available from MGS Research Inc. The manufacture of BANG gel has been described and this gel then became known as PAG gel. PAG is an acronym of polyacrylamide gel. However these systems are also not ideal. They require manufacture, storage and irradiation in hypoxic conditions, specifically a nitrogen environment, because oxygen inhibits the polymerisation reaction.

More recently, normoxic polymer gels have been developed which are made under normal atmospheric conditions (De Deene *et al* 2002). One such gel consists of methacrylic acid,

ascorbic acid, hydroquinone, copper sulphate and gelatin, given the acronym MAGIC (methacrylic and ascorbic acid in gelatin initiated by copper) (Fong *et al* 2001). These gels also have limitations; the methacrylic acid causes degradation of the gelatin matrix over time that leads to poor temporal and spatial stability. A normoxic PAG gel was developed which has a high degree of spatial stability over time. This gel became known as PAGAT, an acronym of PAG and tetrakis (hydroxymethly) phosphonium chloride (Venning *et al* 2004). Polymer gels such as these are now most commonly used for gel dosimetry.

2.1.3 PRESAGE

A new class of dosimeter known as PRESAGE™ has been produced more recently (Heuris Pharma, Skillman NJ, USA), (Adamovics *et al* 2006). PRESAGE is a solid dosimeter, based on transparent polyurethane combined with the leuco-dye leucomalachite green. The dosimeter is designed to absorb strongly at a wavelength of 632 nm in order to be compatible with a He:Ne laser-based scanning system. PRESAGE has a number of potential advantages over both conventional polymer gels and Fricke gels. These include: (i) PRESAGE is a robust solid and needs no container; this makes optical matching and general handling much easier. (ii) Irradiated regions of PRESAGE exhibit negligible diffusion of the coloured medium. (iii) Provided the sample is kept away from light, except while scanning, it appears highly stable (Doran *et al* 2004). PRESAGE is also easy to machine in any desired shape.

2.2 Readout methods

As well as improvements to different dosimeter formulations, an important part of the 3 dimensional dosimetry system is its ability to image the radiation-induced changes in the gel dosimeter. There are now several different imaging modalities for gels that have been demonstrated to be capable of imaging clinically relevant dose distributions, however they all suffer from a number of difficulties. These techniques include ultrasound, x-ray computed tomography and vibrational spectroscopy. The two main evaluation techniques, MRI and optical CT, are discussed here.

2.2.1 Magnetic resonance imaging

MRI was the first proposed as an evaluation method for gel dosimeters by Gore *et al* in 1984. Using the ferrous sulphate chemical dosimeter it was found that the conversion of ferrous to ferric ions by ionising radiation alters the magnetic moment of the metal ion. As a result the spin relaxation times (T1 and T2) of the hydrogen nuclei in the aqueous gel are reduced (De Deene 2004b). In polymer dosimeters, the radiation induced polymeric structures affect the mobility of the surrounding water molecules, thereby affecting the NMR spin-spin relaxation rate, R2 (=1/T2). The relaxation times are obtained by applying a radio frequency (RF) pulse that excited the magnetisation of the spin system. The magnetisation is then sampled as it returns to the equilibrium state.

To date, MRI has been the dominant imaging modality for gel dosimetry, but it is not always practical due to the lack of available scanner time. MRI images may also have image artefacts and the signal to noise ratio can be poor, (De Deene 2004b).

2.2.2 Optical computer tomography

Optical evaluation of Fricke-XO gel dosimeters is possible because of the change in optical absorbance resulting from the formation of the Fe^{3+}-XO complex. Optical CT is similar in principle to x-ray CT, with a light source replacing the x-ray source, and attenuation due to changes in optical absorbance as opposed to density-dependent x-ray attenuation. In parallel beam optical CT, multiple images are taken of the intensity distribution in a broad parallel light beam after it has passed through the gel. The light source can be a light emitting diode (LED) that is used to illuminate a rotating tank containing the gel dosimeter. The attenuated light is projected by lenses onto a CCD detector and images are recorded as the gel dosimeter is rotated. These projections are then used to reconstruct tomographic images of optical attenuation in the gel. This system is able to acquire images relatively quickly, (70 minutes), (Krstajić and Doran 2006).

A second method of optical CT involves a laser scanning system coupled to a photodiode detector (Gore *et al* 1996). Typically a He-Ne laser is used; mirrors mounted on a translating stage are used to scan the laser across a gel as it is rotated. A reconstruction of the irradiated gel is then possible. Advantages of this method include high dynamic range and accuracy when compared to the broad beam source and CCD detector (Krstajić and Doran 2006).

Optical CT has many advantages over MRI including the relatively low cost of a system, simple equipment and technology and a better signal to noise ratio. Doran and Krstajić (2006) provide a comprehensive overview of the history and principles of optical CT for scanning 3 dimensional radiation dosimeters.

3 METHOD

3.1 Preparation of gel

Fricke gel dosimeters can be manufactured using standard chemical laboratory equipment.

Fricke gels (FSX) used at NPL have the following composition: 0.5 mM ferrous ammonium sulphate, 0.1 mM xylenol orange and 25 mM sulphuric acid.

A detailed procedure used for the preparation of Fricke gels as used in this work is given in Appendix A.

3.2 Irradiations

To characterise the gel, several cuvettes of gel were made up on different days and a series of irradiations performed. Irradiations were carried out using either the “Theratron” or “Hotspot 3000” irradiator, as described below.

The Theratron is a typical Co-60 teletherapy unit. Theratron irradiations using a Co-60 gamma ray source were carried out in a water phantom. The dose rate was determined using two NPL 2611 secondary standard ionisation chambers. Measurements were made to ensure that centre of the Fricke gel was positioned at the same point as the reference point of the ionisation chamber.

With each set of irradiations at least one cuvette was kept as an unirradiated control. Each cuvette was covered with a small piece of plastic held in place by tape to ensure no water could enter the gel. The cuvettes were placed in a reproducible upright position in the water phantom in the radiation field on a specially made holder. The irradiation temperature of each cuvette was assumed to be that of the water. Each cuvette was left in the phantom for 5 minutes before the irradiation to reach the water temperature. Typical doses given to the cuvettes range from 5 - 25 Gy, at a dose rate of approximately 1 Gy/min. The overall uncertainty in dose was estimated to be ±1.5% (k=2). After irradiation, the cuvette is dried before being placed in the spectrophotometer for readout.

Irradiations were also undertaken in the Hotspot 3000, one of the NPL's three ^{60}Co self-shielded irradiators. This unit has a dose rate of approximately 20 Gy/min (May 2006) and as such all irradiations were a minute or less in duration. All irradiations in the Hotspot 3000 are dry irradiations with the cuvettes positioned in the centre of the sample compartment. Due to the short irradiation time the irradiation temperature was not controlled. Samples were taken directly from the temperature controlled measurement laboratory (22 ± 2 ^{o}C) for irradiation and this temperature can be considered the irradiation temperature. Overall dose uncertainties are approximately ±3% (k=2).

3.3 Spectrophotometry of the FSX gel

High performance Cary 300 and Cary 3E UV-Vis spectrophotometers were used for absorbance measurements. Both the Cary 300 and Cary 3E spectrophotometer sample holders can accommodate up to six 1 cm cuvettes at any one time. Data collection, including cell movement and repeat acquisition at prescribed time intervals, has been automated using the Varian Application Development Language (ADL).

Each cuvette is read before and after irradiation to enable the change in absorbance to be measured. Full scans of the Fricke gel are acquired as well as individual readings at 543 nm and at 586 nm. 543 nm is the wavelength at which the change in absorbance with dose is most linear, and 586 nm corresponds to the peak of the absorbance spectrum. The full scan range used is 400 – 650 nm.

3.4 Refractive index of FSX gel

The refractive index of two samples of Fricke gel was measured by the NPL Photonics group at the sodium wavelength of 586 nm using an Abbe refractometer. One sample was unirradiated and the other had received ~30 Gy i.e. the maximum usable dose. Ten readings were made for each sample, with the sample repositioned between each measurement. The unirradiated sample was illuminated from above, the sample irradiated to 30 Gy was too opaque to illuminate from above and so was illuminated from below.

For the unirradiated sample the refractive index was measured to be 1.3416, with a standard deviation of 0.0004. The refractive index of the fully irradiated sample was measured to be 1.3418, with a standard deviation of 0.0002. Therefore there is no significant change in refractive index on irradiating the FSX gel.

4 OPTICS

4.1 Set-up

A schematic view from above of the apparatus for the optical CT measurements is shown in figure 1.

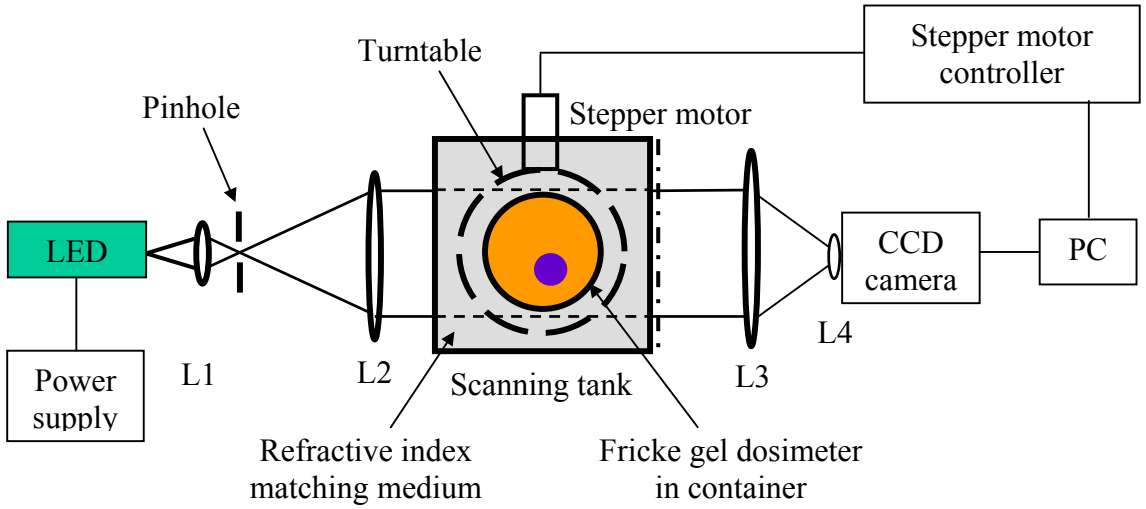

Figure 1. A typical optical CT layout
(Krstajić and Doran 2006)

The apparatus currently being developed at the NPL is similar to the set-up used and described by the University of Surrey (Krstajić and Doran 2006, Krstajić and Doran 2007). The LED light source can be either Amber at 590 nm (part number LXHL-ML1D, Luxeon Star, 1W, Lumileds, California, USA) or Green at 530 nm (part number LXHX-LM5C, 5W, as before), chosen to coincide with the most useful part of the absorbance spectrum of the FSX gel dosimeter. The LED is positioned behind a small lens (LA1951 BK7 plano-convex lens, 25.4 mm focal length, 25.4 mm diameter, Thorlabs Ltd), L1, which is set behind a variable size pinhole. Both the LED and small lens are mounted on a piece of optical rail and their positions can be easily adjusted. These components are kept inside an aluminium box.

The pinhole should be placed at the focal distance of lens L2. Lens L2 creates a parallel beam, which passes through the FSX gel dosimeter, matching medium and scanning tank. The beam is attenuated on passing through the FSX gel dosimeter. The emerging beam is focused by lens L3 onto the camera lens L4 and the CCD camera chip of pixel size 1392 x 1040 (Coolview FDI camera). The image recorded by the camera is that as shown by the dashed-dotted line in figure 1.

The FSX gel dosimeter is placed on a turntable inside the scanning tank. The tank is made from PMMA but the two sides that the beam must pass through are made from polished glass. The tank also contains a matching medium liquid. The turntable is controlled by a stepper motor (model PK264-03B, Oriental Motor Company) that is operated by a stepper motor controller (model BSC001, Thorlabs), controlled by software on the PC. The stepper motor rotates the turntable and FSX gel dosimeter and the CCD camera takes images via the framegrabber card.

The LED/pinhole box, L2, the scanning tank and stepper motor, L3, L4 and the CCD detector are all mounted on an optical rail on the laboratory bench so the positions of all components can be adjusted.

4.2 Matching medium

A matching medium is a solution to match the refractive index of the gel in order to minimise the effect of differences between the refractive indices of Fricke gel, the cylindrical gel holder and the glass walls of the scanning tank (Oldham and Kim 2004). Possible solutions for matching media are sucrose-water solutions with refractive index approximately 1.33 to 1.49, or sodium chloride solutions, refractive index approximately 1.33 to 1.64. Doran *et al* (2001) used a sucrose-water solution. It is important to have a stable solution. In principle it would be possible to colour both a sucrose-water or sodium chloride solution to match the absorbance values of the test phantom or FSX gel.

4.3 Test phantom

It is planned to build a test phantom for validation and QA of the optical CT system. It needs to be a solid material ideally with absorbance at the wavelengths of interest matching that of the gel. The FSX gel is not irradiated uniformly so has regions within it of different dose and hence different optical absorbance, ranging from that of an unirradiated gel to that of a fully irradiated gel. The test phantom is envisaged to be a volume of material with areas of different absorbance to mimic the variation in dose across the gel and enable determination of the spatial and dosimetric resolution. One possibility is to construct the test phantom from dyed PMMA.

Although the refractive index of the test phantom does not need to match that of the FSX gel, it still needs to have a matching medium liquid with refractive index matching that of the test material. The refractive index of PMMA is approximately equal to 1.495.

5 SOFTWARE

There are two parts to the optical CT software; tomography software to control the stepper motor and camera and reconstruction software written in IDL to reconstruct the acquired images. Appendix B describes the tomography program.

The application IDL 6.2 is required to run the reconstruction programs. A book ‘Principles of Computerised Tomographic Imaging’ (Kak and Slaney 2001) is recommended to understand the reconstruction algorithms. NPL currently has a shared licence for IDL. The reconstruction software is made up of a series of IDL procedures and a main image reconstruction program. Full details of the program are given in Appendix C.

6 RESULTS

6.1 Cuvette irradiations

The Fricke gel cuvettes were irradiated to nominal doses of 5, 10, 15 and 20 Gy in either the theratron or Hotspot 3000 irradiator (see 3.2). The absorbance as a function of

wavelength was read out by the Cary 300 UV-Vis spectrophotometer. The spectrophotometer was programmed to take a reading of absorbance on each cuvette over the wavelength range 400 – 650 nm in 1 nm steps. The measurement was repeated every 10 minutes for a total of 24 hours. Figure 2 shows the absorbance as a function of wavelength for both unirradiated and irradiation gels immediately after irradiation and 10 hours later. The cuvettes were irradiated, measured and stored in the Cary 300 at 22 ± 2 ^{o}C.

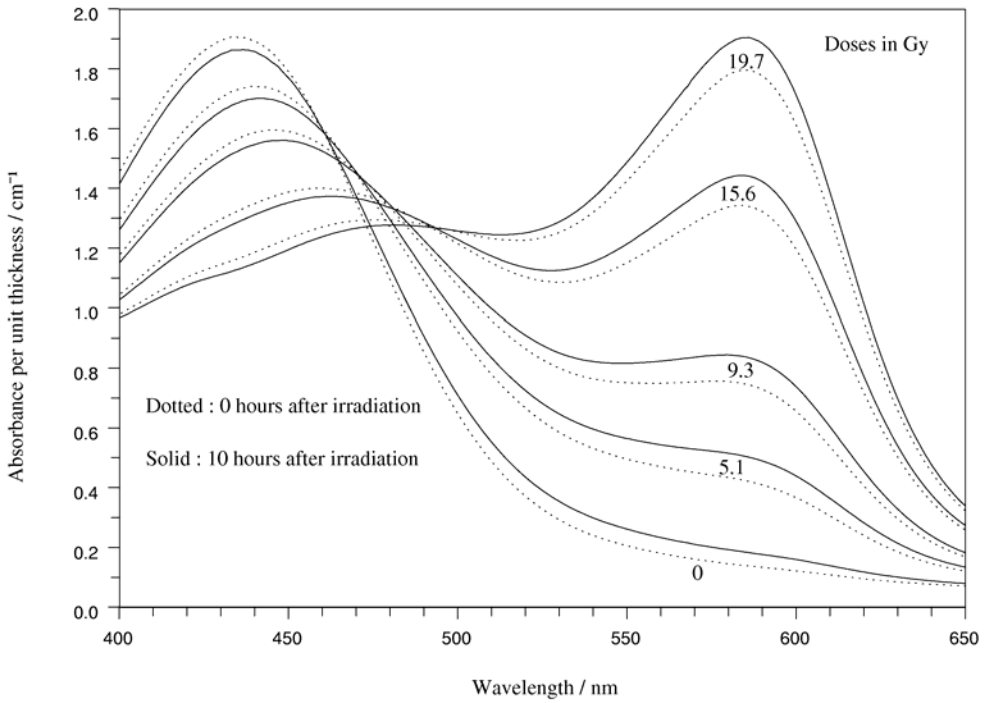

Figure 2. Absorbance as a function of wavelength for a range of doses at 0 and 10 hours after irradiation

The two wavelengths of interest are those at 543 nm, where the increase in total absorbance is approximately linear with dose, and 586 nm, which corresponds to the greatest total absorbance. The total absorbance at each of these wavelengths as a function of dose is shown in figures 3 and 4 for measurements made at 0 and 10 hours after irradiation.

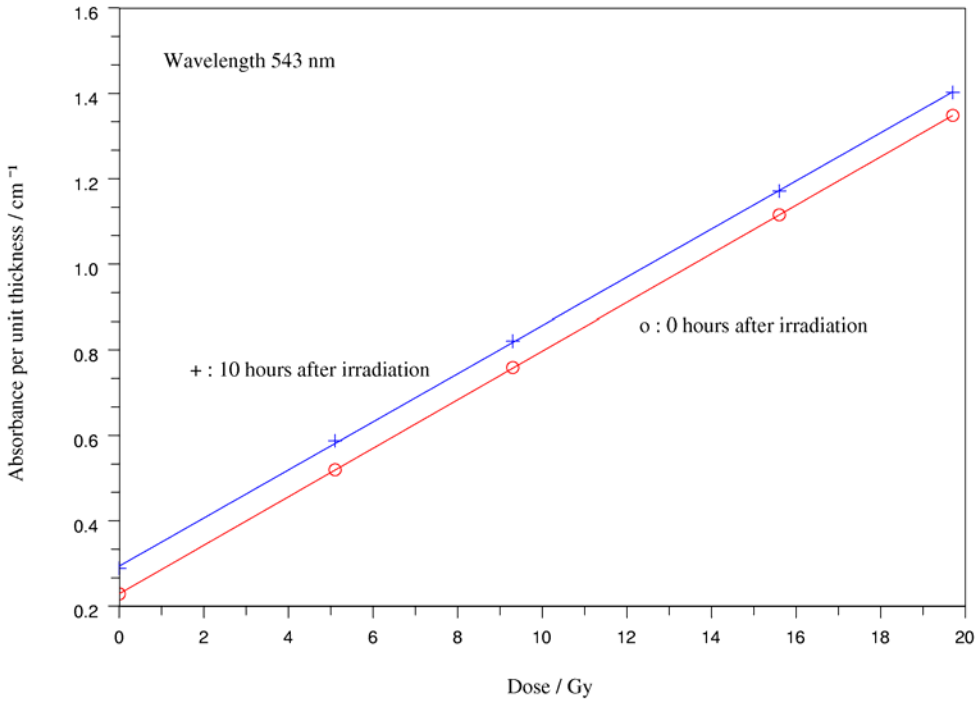

Figure 3. Absorbance as a function of dose at 0 and 10 hours after irradiation: 543nm

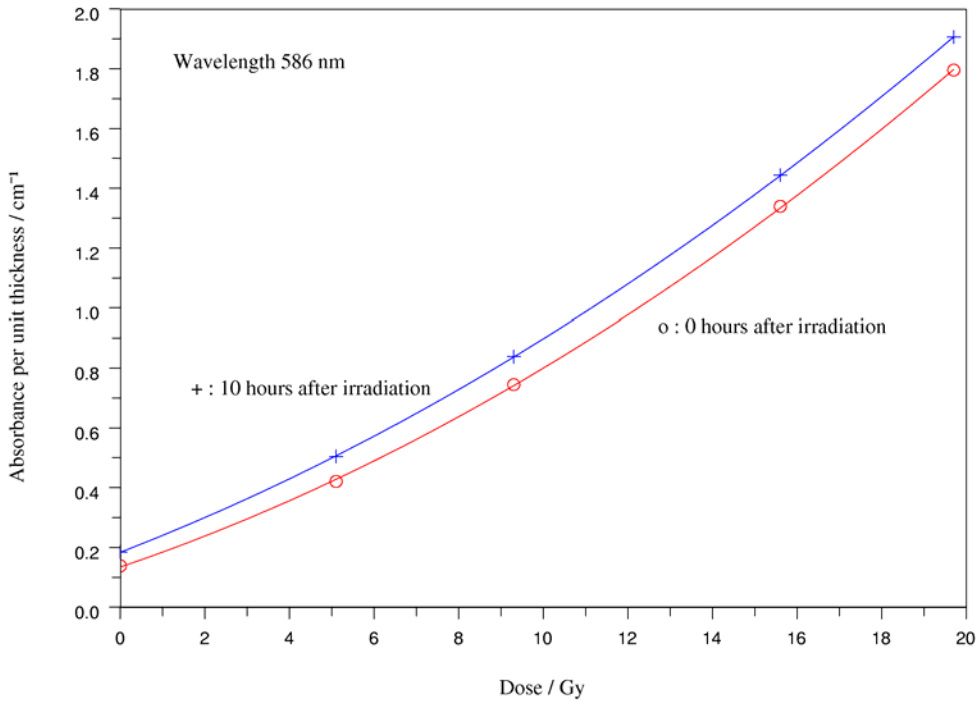

Figure 4. Absorbance as a function of dose at 0 and 10 hours after irradiation: 586nm

The absorbance as a function of time was measured for each gel, with a measurement and storage temperature of 22 ± 2 ^{o}C. The change in absorbance with time was then converted

in to an equivalent change in dose, using the calibration curves in figures 3 and 4. This enables the drift with time to be quantified and can be used in an uncertainty evaluation.

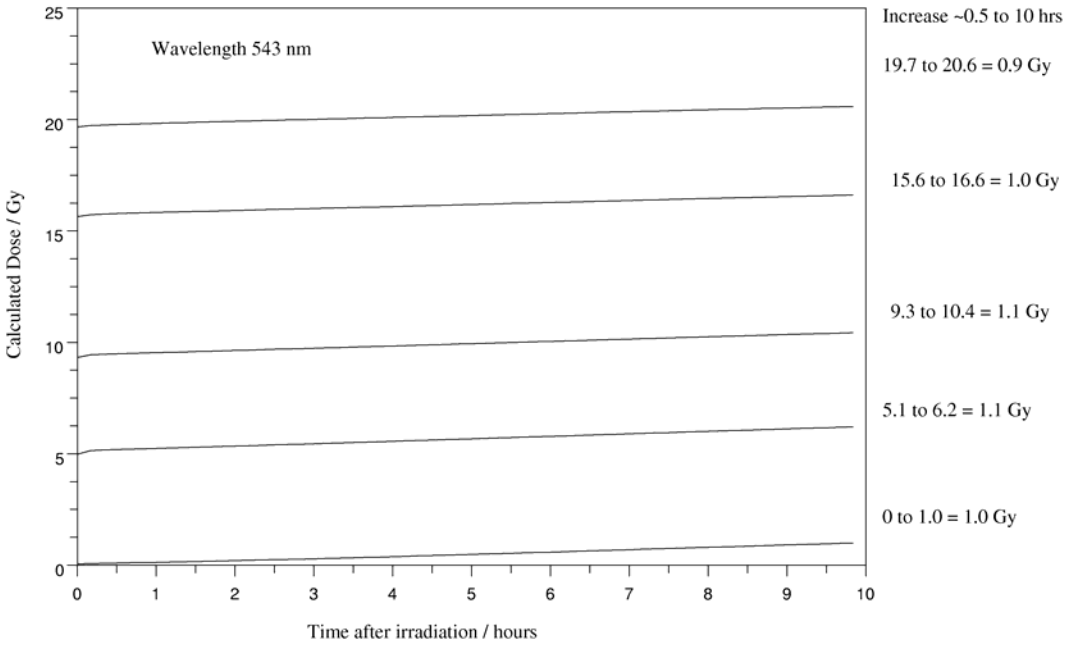

Figure 5. Change in measured dose with time for doses between 0 and 20 Gy: 543nm

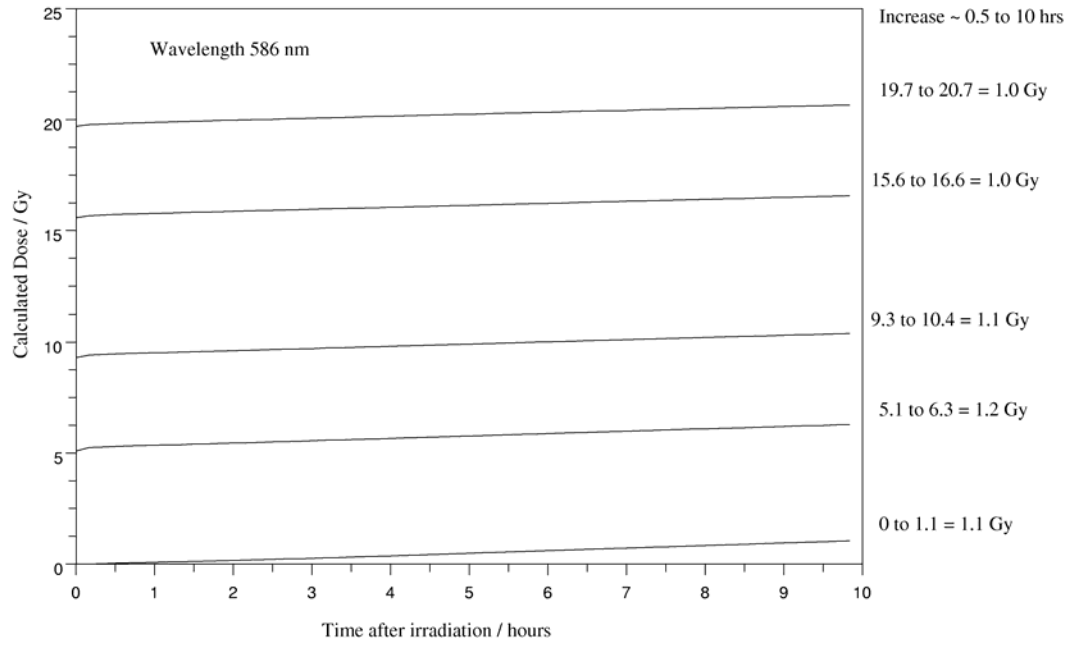

Figure 6. Change in measured dose with time for doses between 0 and 20 Gy: 586nm

6.2 Gel response at lower temperatures.

The changes in absorbance with time reported above could potentially be reduced by maintaining the gels at lower temperatures. To investigate this effect, gel cuvettes were irradiated to nominal doses of 5, 10, 15, 20 Gy at an irradiation temperature of 17 ± 2 °C. These samples were then stored at 10 ± 2 °C in the spectrometer and measured at 10 minute intervals from 0 to 10 hours after irradiation.

The absorbance as a function of time was measured for each gel, with a measurement and storage temperature of 10 ± 2 °C. The change in absorbance with time was then converted in to an equivalent change in dose, using the calibration curves in figures 3 and 4, and is displayed in figure 7.

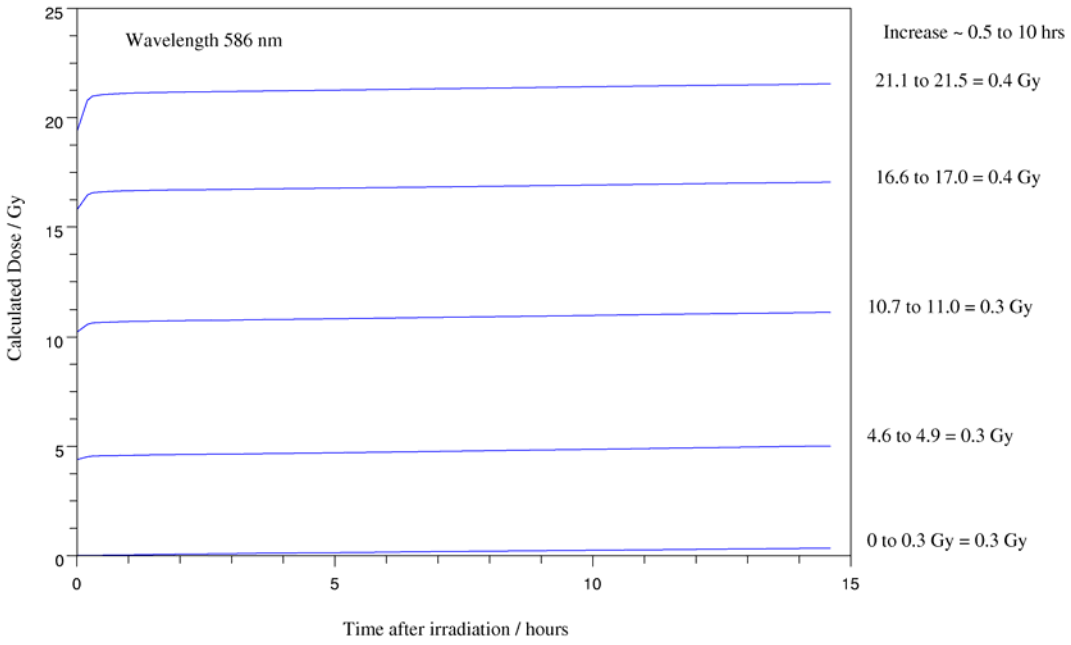

Figure 7. Change in measured dose with time for doses between 0 and 22 Gy at 586 nm for gel measured at 10 ± 2 °C.

Table 1 shows a comparison of the increase in absorbance (expressed in terms of measured dose) in the first 0.2 hours after irradiation for gels stored at 10 ºC and 22 ºC. Figure 8 shows graphically the increase in measured dose over a period up to 10 hours after irradiation for samples irradiated to ~20 Gy and stored at 10 ºC and 22 ºC. The results shown are for 586 nm, but similar rates of change were observed at 543 nm.

Wavelength (nm)	543	586	543	586
Nominal Dose (Gy)	Nominal measurement / storage temperature 10 °C		22 °C	
	Increase in measured dose from 0 to 0.2 hour measurement Gy			
0	0.00	0.01	0.01	0.01
5	0.13	0.13	0.16	0.16
10	0.34	0.35	0.12	0.12
15	0.67	0.66	0.09	0.09
20	1.41	1.42	0.08	0.07

Table 1. Comparison of increase in measured dose over a period 0.2 hours for samples stored at 10 and 22 °C.

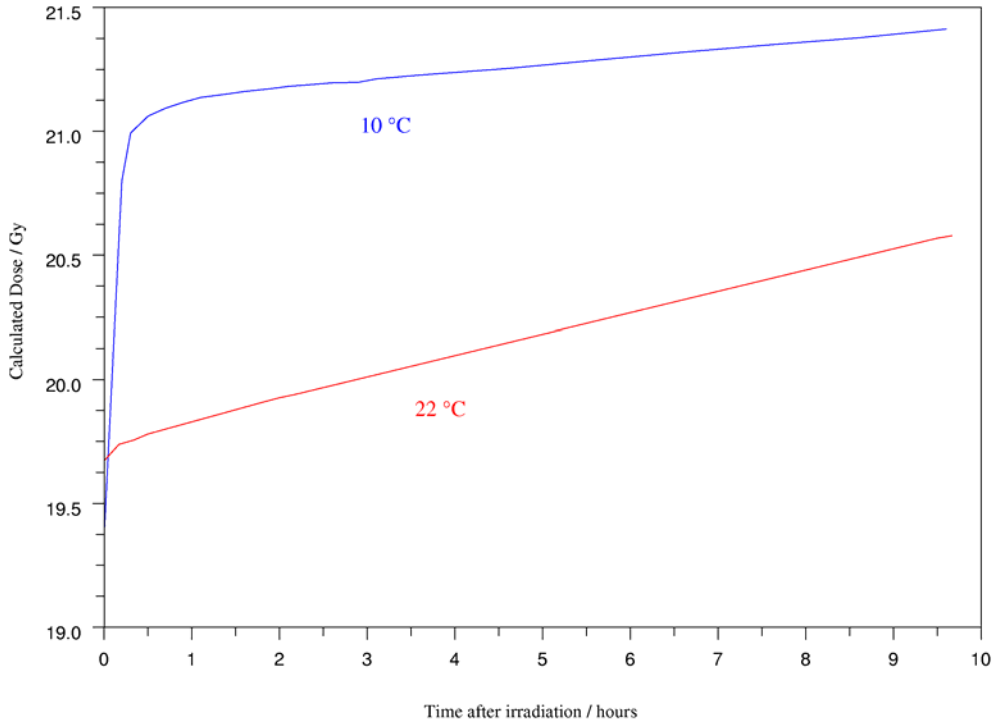

Figure 8. Increase in measured dose over a period of 10 hours after irradiation for samples stored at 10 ºC and 22 ºC.Doses in each case were ~20 Gy, but were not equal. Data shown is for measurements made at 586 nm.

6.3 Reproducibility of unirradiated gel

The absorbance values of unirradiated samples taken from a number of different batches of gels prepared at NPL are summarised in Tables 2 and 3. Also shown are the equivalent mean background doses, calculated using the calibration data given in Figs 3 and 4, and their standard deviations and ranges. The exact time of measurement after removing a cuvette from the fridge is not known in all cases and this may account for some of the variation seen between batches. Results only include those for gels measured and stored at 22 ± 2 °C.

Date	No of cuvettes	Mean absorbance (cm^{-1})	Mean effective background dose (Gy)	St dev (Gy)	Background dose range (Gy)
14/06/2002	10	0.1593	2.80	0.21	0.76
27/06/2002	12	0.2077	3.66	0.37	1.11
05/07/2002	15	0.2480	4.37	0.47	1.25
11/07/2002	10	0.2425	4.27	0.32	1.12
06/08/2002	12	0.2351	4.14	0.07	0.23
08/07/2005	16	0.2029	3.57	0.08	0.32
12/07/2005	7	0.1937	3.41	0.05	0.13
09/03/2006	4	0.2180	3.84	0.04	0.08
04/05/2006	5	0.2284	4.02	0.04	0.10

Table 2. Effective background dose of unirradiated gel samples: 543 nm

Date	No of cuvettes	Mean absorbance (cm^{-1})	Mean effective background dose (Gy)	St dev (Gy)	Background dose range (Gy)
14/06/2002	10	0.1046	2.09	0.13	0.44
27/06/2002	12	0.1325	2.65	0.23	0.78
05/07/2002	15	0.1533	3.07	0.40	1.07
11/07/2002	10	0.1511	3.02	0.29	0.99
06/08/2002	12	0.1442	2.88	0.06	0.18
08/07/2005	16	0.1212	2.42	0.07	0.30
12/07/2005	7	0.1129	2.26	0.05	0.15
09/03/2006	4	0.1312	2.62	0.04	0.08
04/05/2006	5	0.1377	2.75	0.04	0.10

Table 3. Effective background dose of unirradiated gel samples: 586 nm

6.4 Reproducibility of radiation response

For each batch of FSX gel, cuvettes were irradiated to a range of doses between 1 - 50 Gy. The actual doses varied from batch to batch and so a comparison between batches is most clearly seen graphically. The change in optical absorbance per centimetre as a function of dose for gels from different batches is shown in figures 9 and 10. A different batch of gel was prepared and irradiated on each date.

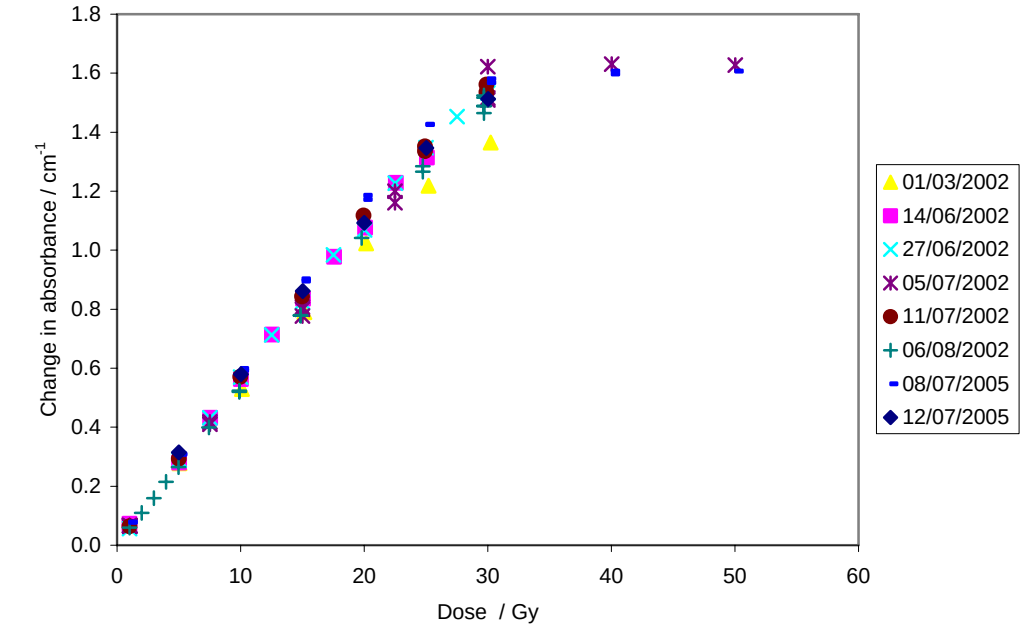

Figure 9. Change in absorbance as a function of dose for different batches: 543nm

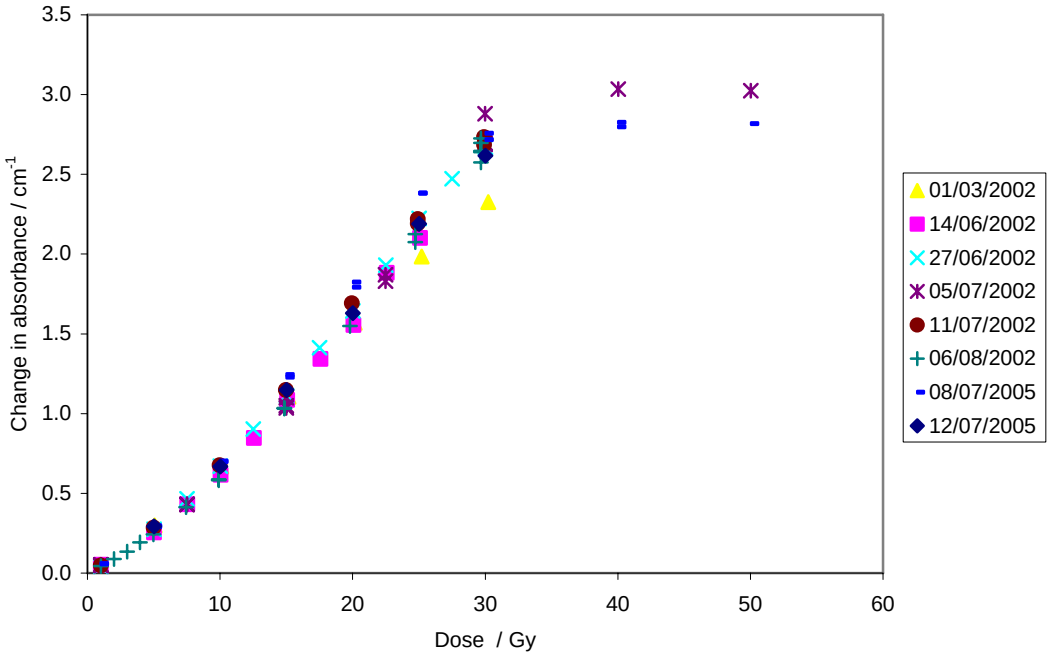

Figure 10. Change in absorbance as a function of dose for different batches: 586nm

6.5 Cuvettes of gel held in normal light and darkness.

Four un-irradiated cuvettes were compared after twenty-four hours held either in laboratory light or in darkness. Results from these experiments show that those samples kept in the dark are approximately 0.3 Gy lower (at 543 nm and 586 nm) in effective dose than those kept in the light. It should be emphasised these results are based on only a few cuvettes and as such some of this effect may be due, in part, to cuvette to cuvette variation.

6.6 Plugs of gel from the circular holder

To investigate cooling within the gel body cuvette sized samples were removed from the block and the absorbance measured. The gel was made up as described and left to set in the fridge over night. The next day the block was removed from the fridge and cuvettes were used as ‘plugs’ to sample a cuvette sized piece of gel. Before use a small hole was drilled through the base of the cuvette. The approximate location of these 'plugs’ was as shown in figure 11.

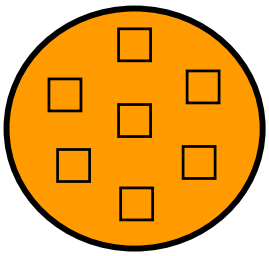

Figure 11. Plugs of gel from the block

The absorbance of the central plug and two outside plugs was compared before irradiation. Three outside plugs and the central plug were then irradiated to approximately 15 Gy and their absorbance measured and compared. The results are shown in table 4. The difference is given as an effective dose between the maximum and minimum absorbance values.

	Wavelength (nm)	Mean absorbance (cm^{-1})				Difference
		Centre	Outside 1	Outside 2	Outside 3	
Unirradiated	543	0.2024	0.2061	0.2063	-	0.07 Gy
	586	0.1189	0.1205	0.1206	-	0.03 Gy
Irradiated	543	1.0648	1.0823	1.0775	1.0878	0.42 Gy
	586	1.2719	1.3075	1.2989	1.3154	0.47 Gy

Table 4. Absorbance of the plugs of gel

7 DISCUSSION

7.1 Cuvette irradiations

Figure 2 shows the change in absorbance with dose at different wavelengths. At wavelengths less than 480 nm the absorbance decreases as the dose is increased, and above this wavelength the absorbance increases with dose.

Figures 3 and 4 show the optical absorbance per centimetre as a function of dose for the wavelengths 543 nm and 586 nm respectively. For 543 nm it can be seen that the increase in absorbance with dose is close to being linear. The increase is not linear for 586 nm.

Figures 2 to 6 all show optical absorbance measurements made both immediately and several hours after irradiation. Figures 2 to 4 show a significant increase in absorbance ten hours after irradiation and figures 5 and 6 show how the absorbance changes with time

during this period. The increase is equivalent to approximately 1 Gy over 10 hours for gels stored at 22 ºC and is essentially independent of given dose. It is likely that an irradiated gel would be read out within 2 hours of irradiation and so the observed change in dose would be of the order of 0.2 Gy.

7.2 Gel response at low temperatures

Comparing the response of the low temperature (~10 ºC) experiment to earlier experiments at irradiation, measurement and post-irradiation temperatures of ~22 ºC, the cooling of the samples appears to have two effects, both of which can be seen graphically in figure 8.

a) Slowing of the initial short-term changes.

With the higher temperature experiment all initial radiation induced changes were complete before the second measurement i.e. within 10 minutes. With the lower temperature experiment it was possible to see dose dependent, changes up to nearly 30 minutes post irradiation. A comparison of this data is tabulated in table 1.

b) Slowing of long-term changes.

After the initial changes both curves in figure 8 show a gradual increase in measured dose with time, but the change is significantly smaller at the lower temperature. Figures 5 - 7 show that at both temperatures, the change in measured dose over ten hours is independent of the given dose. From 0.5 hours post irradiation until about 10 hours post irradiation the high temperature experiments show an increase in dose of about 0.1 Gy/hour whereas over a similar period those kept at 10 ^{o}C only show an increase of about 0.03 Gy/hour. In all cases the measurement wavelength does not appear to affect the results.

7.3 Reproducibility

Figures 9 and 10 show the change in absorbance per unit thickness between the unirradiated and irradiated gels as a function of dose for measurements made for different batches, for wavelengths of 543 nm and 586 nm. It can be seen that the points from different days all follow the same basic shape for each wavelength. Tables 2 and 3 show the reproducibility within batches of unirradiated gel. The data indicates that as more batches were made the reproducibility improved, although this may be due to more rigid measurement, storage conditions and readout times. It was not always clear whether cuvettes had been consistently read out under the same conditions, so this may be reflected in the differences between maximum and minimum optical absorbance values within a batch.

The range in effective background dose within each batch of unirradiated gel samples is of the order of 1 Gy. This is the maximum difference in measured dose that will arise from variability in unirradiated samples within a given batch of gel.

7.4 Samples of gel from the circular holder

Table 4 shows the absorbance per unit thickness at 543 nm and 586 nm and the difference in effective dose between the maximum and minimum readings for samples taken from the gel block. This was done for both unirradiated and irradiated cuvettes. The difference

between the central plug and those at the outside are better than 0.1 Gy for the unirradiated cuvettes and better than 0.5 Gy for the samples irradiated to approximately 15 Gy.

8 CONCLUSION

Measurements have been made to characterise the FSX gel made at the NPL for use in the optical CT gel dosimetry system. From the results presented here it would appear that 543 nm is the optimum wavelength at which to carry out optical absorbance measurements on the gel. At this wavelength there is an almost linear dependence of optical absorbance per unit thickness with absorbed dose. This is most useful in calculating absorbed dose from optical absorbance. The developing time of the gel is also similar for both 543 nm and 586 nm. 586 nm corresponds to the peak of the optical absorbance spectrum. This wavelength is useful because the change in absorbance on irradiation is greatest here, however the increase in absorbance with dose is not as linear at this wavelength.

The work reported at lower temperatures demonstrated that both short and long term increases in optical absorbance and hence measured absorbed dose were slowed. The developing time of the Fricke gel, shown through the initial short-term changes, is longer at the lower temperature, as reaction rates within the gel are slower. The longer term increase in absorbance is also slower for the lower temperature measurements. These measurements indicate that for increased stability the Fricke gel should be stored and measured at the lower temperatures (10 ± 2 ^{o}C), but left for 30 minutes before readout to enable developing of the colour within the gel to take place. Lower temperatures may also reduce diffusion of the Fe^{3+}-XO complex in the gel, enhancing the spatial resolution.

The range of effective background doses of samples within a batch of gel was initially ~1 Gy, although improvements in the manufacture of the gel since 2005 have decreased this range to less than 0.4 Gy. This will contribute to the variability of doses measured in irradiated samples and needs to be taken into account in preparing an uncertainty budget.

No significant difference was observed in either irradiated or unirradiated sample plugs taken from different parts of the gel. This implies that the method of preparation and cooling described here is effective in producing gels of uniform response throughout the volume. The difference in absorbance between plugs over the gel body were similar to those expected due to variations within a batch.

For future reference, it is important to record carefully conditions under which the gel was both manufactured and kept before and after irradiation to enable a more accurate comparison within a batch and between batches. The observed absorbance per unit thickness is dependent on the time between irradiation and measurement. This may account for some of the large differences observed between batches in figures 9 and 10.

The optics system is currently under development by the Photonics Group at NPL. A suitable matching medium must be identified for use with the system.

Software for both image acquisition and reconstruction detailed in this Report has been run successfully. Improvements to the software have already been investigated; in particular the Scilab program has been improved by the addition of compiled code (Toft 1996).

9 REFERENCES

Adamovics J, Jordan K and Dietrich J 2006 PRESAGE™ - Development and optimization studies of a 3D radiochromic plastic dosimeter – Part 1 *J. Phys.: Conf. Ser.* **56** 172-175

Adamovics J, Guo P, Burgess D, Manzoor A and Oldham M 2006 PRESAGE™ - Development and optimization studies of a 3D radiochromic plastic dosimeter – Part 2 *J. Phys.: Conf. Ser.* **56** 176-178

Appleby A and Leghrouz A 1990 Imaging of radiation dose by visible color development in ferrous-agarose-xylenol orange gels *Med. Phys.* **18** 309-312

Attix F H 1986 *Introduction to Radiological Physics and Radiation Dosimetry* (J. Wiley and Sons)

Bero M A, Gilboy W B, Glover P M and Keddie J L 1999 Three-dimensional radiation dose measurements with Ferrous Benzoic Acid Xylenol Orange in Gelatin gel and optical absorbance tomography *Nucl. Inst. Meth. A* **422** 617-620

De Deene Y, Hurley C, Venning A, Vergote K, Mather M, Healy B J and Baldock C 2002 A basic study of some normoxic polymer gel dosimeters *Phys. Med. Biol.* **47** 3441-3463

De Deene Y 2004a Essential characteristics of polymer gel dosimeters *J. Phys.: Conf. Ser.* **3** 34-57

De Deene Y 2004b Fundamentals of MRI measurements for gel dosimetry *J. Phys.: Conf. Ser.* **3** 87-114

Doran S J, Koerkamp K K, Bero M A, Jenneson P, Morton E J and Gilboy W B 2001 A CCD-based optical CT scanner for high-resolution 3D imaging of radiation dose distributions: equipment specifications, optical simulations and preliminary results *Phys. Med. Biol.* **46** 3191-3213

Doran S J, Krstajić N, Adamovics J and Jenneson P M 2004 Optical CT scanning of PRESAGE™ polyurethane samples with a CCD-based readout system *J. Phys.: Conf. Ser.* **3** 240-243

Doran S J and Krstajić N 2006 The history and principles of optical computed tomography for scanning 3-D radiation dosimeters *J. Phys.: Conf. Ser.* **56** 45-57

Fong P M, Kel D C, Does M D and Gore J C 2001 Polymer gels for magnetic resonance imaging of radiation dose distributions at normal room temperature *Phys. Med. Biol.* **46** 3105-3113

Fricke H and Hart E J 1966 Chemical Dosimetry *Radiation Dosimetry* vol. 2 F H Attix and W C Roesch (ed.) (New York: Academic Press)

Gore J C, Kang Y S and Schultz R J 1984 Measurement of radiation dose distributions by nuclear magnetic resonance (NMR) imaging *Phys. Med. Biol.* **29** 1189-1197

Gore J C, Ranade M, Maryañski M J and R J Schultz 1996 Radiation dose distributions in three dimensions from tomographic optical density scanning of polymer gels: I. Development of an optical scanner *Phys. Med. Biol.* **41** 2695-2704

Johns H E and Cunningham J R 1983 *The Physics of Radiology* (Charles C Thomas)

Kak A C and Slaney M 2001 *Principles of Computerized Tomographic Imaging*, (Society of Industrial and Applied Mathematics) 49-74
Available online at http://www.slaney.org/pct/

Kelly R G, Jordan K J and Battista J J 1998 Optical CT reconstruction of 3D dose distributions using the ferrous-benzoic-xylenol (FBX) gel dosimeter *Med. Phys.* **25** 1741-1750

Krstajić N and Doran S J 2006 Focusing optics of a parallel beam CCD optical tomography system for 3D radiation gel dosimetry *Phys. Med. Biol.* **51** 2055-2075

Krstajić N and Doran S J 2007 Characterisation of a parallel beam CCD optical tomography system for 3D radiation gel dosimetry *Phys. Med. Biol.* **52** 3693-3713

Maryañski M J, Schultz R J, Ibbott G S, Gatenby J C, Xie J, Horton D and Gore J C 1994 Magnetic resonance imaging of radiation dose distributions using a polymer gel dosimeter *Phys. Med. Biol.* **39** 1437-1455

Mather M L 2003 Ultrasound Evaluation of Radiation Sensitive Polymer Gels *PhD Thesis* School of Physical and Chemical Sciences, Queensland University of Technology

MGS Research Inc., 1 Orchard Park Road, Suite 13, Madison, CT 06443
Oldham M and Kim L 2004 Optical-CT gel-dosimetry II: Optical artifacts and geometrical distortion *Med. Phys.* **31** 1093-1104

Rae W I D, Willemse C A, Lotter M G, Engelbrecht S and Swarts J C 1996 Chelator effect on ion diffusion in ferrous-sulphate doped gelatin gel dosimeters as analysed by MRI *Med. Phys.* **23** 15-23

Schreiner L J 2004 Review of Fricke gel dosimeters *Proc. 3rd Int. Conf. On Radiotherapy Gel Dosimetry* ed. De Deene Y and Baldock C (Ghent, Belgium) 10-22

Schultz R J, deGuzman A F, Nguyen D B and Gore J C 1990 Dose response curves for Fricke-infused agarose gels as obtained by nuclear magnetic resonance *Phys. Med. Biol.* **35** 1611-1622

Tarte B J, Jardine P A, van Doorn T, Nitschke K N and Poulsen M G 1997 Development of a CCD array imaging system for measurement of dose distributions in doped agarose gels *Med. Phys.* **24** 1521-1525

Toft P 1996 The Radon Transform - Theory and Implementation *PhD thesis* Department of Mathematical Modelling, Technical University of Denmark
Available online at http://petertoft.dk/PhD/

Venning A J, Brinda S, Hill B and Baldock C 2004 Preliminary investigation of a novel normoxic PAG gel dosimeter with tetrakis (hydroxymethyl) phosphonium chloride as an anti-oxidant *J. Phys.: Conf. Ser.* **3** 155-158

Venning A J 2006 Investigation Of Radiation Sensitive Normoxic Polymer Gels For Radiotherapy Dosimetry *PhD thesis* School of Physical and Chemical Sciences, Queensland University of Technology

10 APPENDIX A: Procedure for gel preparation

With the exception of the gelatin all chemicals used in the preparation are high purity analytical grade as this system can be very sensitive to impurities. Water in particular constitutes a large percentage of the solution by weight and hence its purity is important. In this work water equivalent to single stilled or better is used throughout.

1. Before use, all glassware must be cleaned using chromic acid and rinsed thoroughly with distilled water.

2. Make up two 1000 ml stock solutions of 25 mM H_2SO_4.

For each 1000 ml solution: A 5 ml measuring cylinder is weighed and the balance zeroed. A pipette is used to measure 2.452 g of H_2SO_4 on a precision balance. Distilled water is added to a 1000 ml volumetric flask and the sulphuric acid is added to this water. The flask is filled up to 1000 ml using distilled water. This process is repeated to make a second 1000 ml volumetric flask of 25 mM H_2SO_4.

3. Make up a stock solution of Fe^{2+} ions.

A white weighing dish is weighed and the balance is zeroed. Using a platinum spatula cleaned by heating in a Bunsen burner 0.392 g of ferrous ammonium sulphate powder is measured then placed in a 100 ml glass beaker. A small quantity of stock sulphuric acid is added to the beaker, the solution is stirred then poured into a 100 ml volumetric flask. Further stock sulphuric acid is added to make the solution up to the 100 ml mark.

4. Make up a stock solution of XO.

A white weighing dish is weighed and the balance is zeroed. The platinum spatula is re-cleaned in the Bunsen burner and 0.760g of xylenol orange powder is placed in a 100 ml glass beaker. A small quantity of stock sulphuric acid is added, the solution is stirred then poured into a 100 ml volumetric flask. Further stock sulphuric acid is added to make the solution up to the 100 ml mark.

5. Make up a stock solution of both Fe^{2+} and XO.

10 cm^3 of the stock XO is measured out using a 10 ml pipette and placed in a 250 ml volumetric flask. 50 cm^3 of the stock Fe^{2+} solution is measured out using a 50 ml pipette and added to the same volumetric flask. The solution is made up to 250 ml by adding 190 cm^3 of H_2SO_4.

6. Add 50 g of gelatin to 750 ml of stock H_2SO_4 solution.

50 g of gelatin is measured on to a clean white weighing dish. The white weighing dish and gelatin are transported inside a 20 cm diameter glass dish and covered by a large watch glass to prevent any gelatin loss. 750 ml of stock H_2SO_4 solution is measured into a 2000 ml glass beaker using a 250 ml or 500 ml measuring cylinder. The gelatin is added to the sulphuric acid and this solution is left for 10-15 minutes in which time the gelatin starts to dissolve in the H_2SO_4.

7. Heat to 45°C and allow to become liquid.

The 2000 ml glass beaker is placed on a hot plate and heated to 45°C. A magnetic stirrer is added to the solution and stirred slowly as the gelatin fully dissolves. It is removed from the heat and allowed to cool to about 32°C while continually being stirred. This takes approximately 37 minutes.

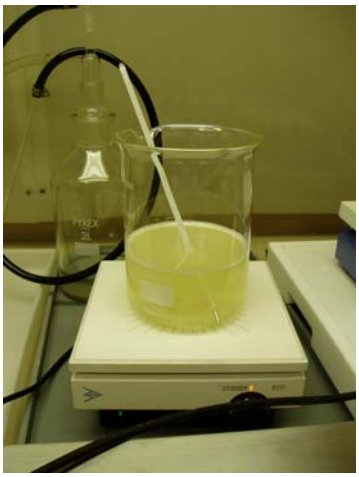

Figure A1. Stirring the heated gelatin/H_2SO_4 solution

8. Add the Fe^{2+}/XO stock solution to the gelatin/H_2SO_4 solution.

The 250 ml solution of Fe^{2+}, XO and H_2SO_4 is poured carefully into the gelatin solution. The magnetic stirrer continues to mix the solutions.

9. Pour solution into holders and store in the fridge.

The irradiations are carried out either in 1 cm path cuvettes for the purpose of determining the characteristics of the gel, or a special gel holder for the 3D irradiations and readout. When fully mixed the solution is carefully poured into either cuvettes or the gel holder. The gel holder is made of plastic tubing with a carefully made base and lid. The base has holes drilled into it to enable positioning on the turntable for the 3D optical readout system. The base is fitted before pouring in the gel and sealed with tape to prevent leakage. Both base and lid are a snug fit. The gels are stored in the fridge.

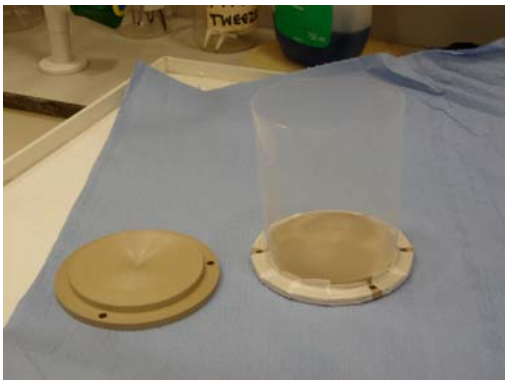

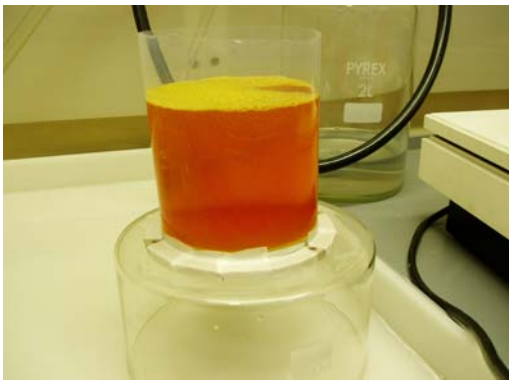

Figure A2. The gel holder

11 APPENDIX B: Tomography program

A visual basic program `gelOCT.exe` is used for data acquisition and rotation control of the stepper motor. It controls both the camera and stepper motor. Running the program `gelOCT.exe` opens the gelOCT window. Select **Acquire** and then **Continuous** to show a live feed from the camera, an example of which is displayed in figure B1.

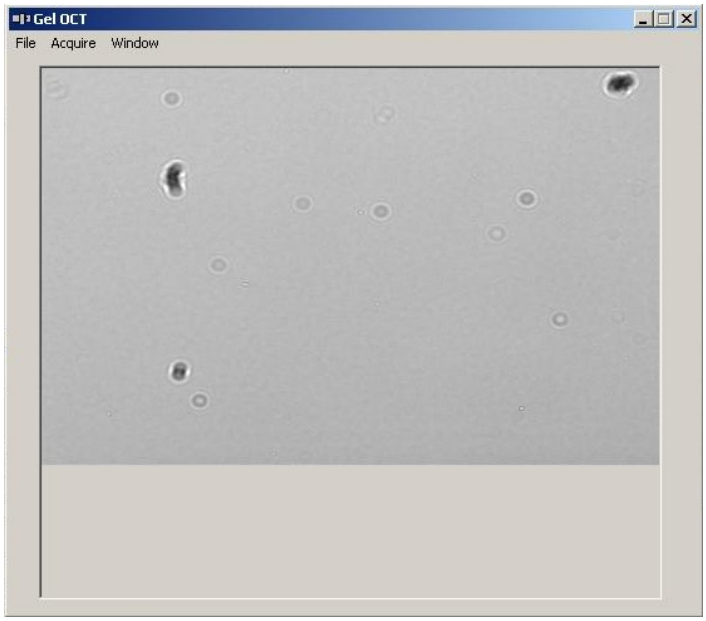

Figure B1. The gelOCT window showing the image recorded by the camera

The **Window** function enables the opening of the Stepper Motor Setup window, as shown in figure B2, or the Tomography control window, as shown in figure B3.

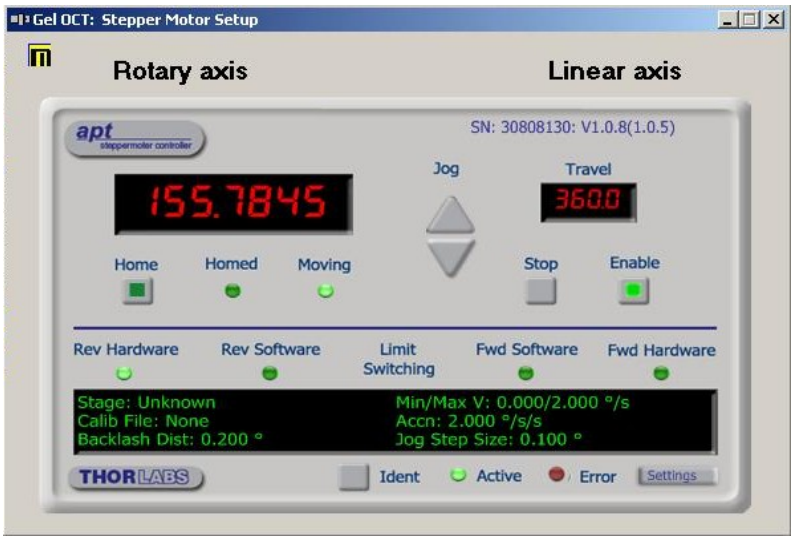

Figure B2. The stepper motor set-up

The Stepper Motor Setup window enables operation of the stepper motor. The motor can be set to return to **Home** or jogged a small increment. The numbers displayed all have

units of degrees. The **Settings** tab can be used to adjust additional settings, such as the maximum and minimum velocity, acceleration, step size and maximum and minimum position.

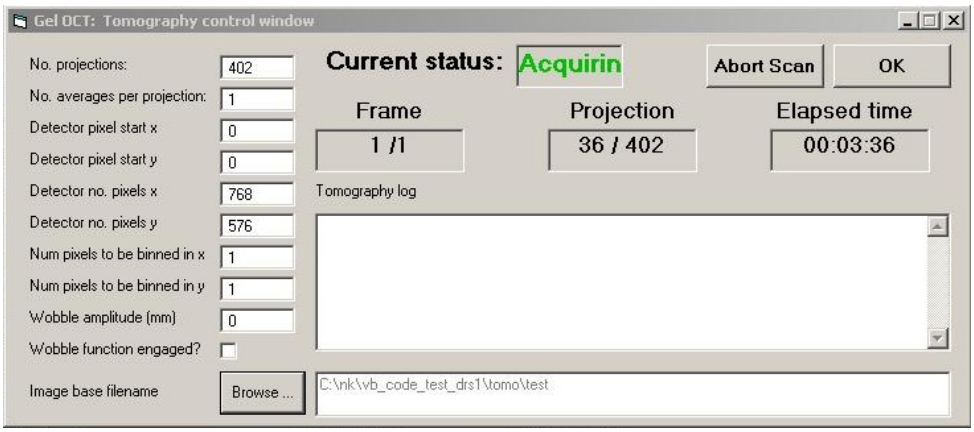

Figure B3. The tomography control window

The tomography control window works alongside the stepper motor to control image acquisition by the camera. With the current settings 402 projections step the motor round and acquire images through 180^{o}. The image base filename must be created before starting acquisition; the program will not run if the filename already exists. To start image acquisition return to the main gelOCT window as shown in figure B1, select **Acquire**, then **Tomographic Scan**. This operates both the stepper motor and camera.

Data files are saved in the form, e.g. *test0xxx.oct* and *test0xxx.oct.tif*. The *.oct* files are those needed for the reconstruction. Files of the type *.oct.tif* are the images themselves and can be viewed using the application *ImageJ* that can be downloaded for free from the internet.

12 APPENDIX C: Reconstruction program

The IDL procedures are in the zipped folder *simon_code.zip*. They must be unzipped into a folder *simon_code*. Copy the program `brachy.pro` into a local folder too.

To run the files open IDL. Within IDL select **File**, **Preferences**, then **Path**. Select the path address to the folder *simon_code* containing these procedures.

All procedures used by IDL must be precompiled. To do this type '`@compile`' in the IDL command line. This needs to be done whenever the software is opened. It opens the scripts.

The scans acquired from the data acquisition program should be saved in a designated folder. Edit the program `brachy.pro` to ensure that the prefix of the data set is correct. If there are any correction files for dark noise ensure these are located too. Create a folder, O*utput*, to which the output files produced by running `brachy.pro` and edit the program to ensure the location of both this folder and that of the data acquisition scans is correct.

Compile and then **Run** `brachy.pro`.

```
;**********************************************************************
**
; Analyse data for optical tomography experiment for 0 OD.
;
; Modified from Simon J. Doran ( which in turn was modified from
recon.pro
; by Koen Klein Koerkamp)       20.05.05
;**********************************************************************
**

pro brachy

    begin_time = systime(1)

    ;-----------------------------------------------------
    ; Collect parameters for reading and processing data.
    ;-----------------------------------------------------

    data_pref    =  'D:\scans\finger\optics_clarity\brachy1\brachy'      ;
prefix of dataset to be processed



    ;corr_file    =  'D:\scans\finger\optics_clarity\milkphantom2'       ;
correction data set
    ;dark_file  = 'D:\scans\finger\optics_clarity\brachy1\dark_field.oct'
; dark image
    out_dir       =  'D:\scans\finger\optics_clarity\brachy1\output\'    ;
output directory

; Get the tomography parameters from the first OCT file.
    proj1                              =                               read_oct(
'D:\scans\finger\optics_clarity\brachy1\brachy0001.oct', header=hdr )

    tvscl, proj1
```

```
    stop
```

Edit these lines for the data to reconstruct. For example, if the output files from the data acquisition are saved as eg. *brachy0024.oct* then the prefix is *brachy*. The *dark_file* is the file recorded by the CCD when the room is dark and is any noise that can be removed. This may or may not be used in the reconstruction analysis. Ensure an output folder is set up for the reconstructed images. This folder must be empty prior to starting the analysis. Enter the full details of the first OCT file to be analysed.

```
    ; Smooth the edge and use it later on as correction scan.
    lf_smooth = fltarr(768)
    lf_raw = proj1[*,560]
    lf_smooth = smooth(lf_raw,70)

    nx     = hdr.n_proj_pix_x
    ny     = hdr.n_proj_pix_y

    ; TO DO: OCT file is not written to correctly! Needs sorting.
    nx = 768
    ny = 560
```

`nx` and `ny` are the size of the image in pixels.

```
    nproj  = 1000 ;hdr.n_proj
    use_wobbledata = 0
```

`nproj` is the number of projections taken to analyse, starting from the one specified at the start of the program.

```
    for slice = 280, 420 do  begin    ; row in images to be backprojected
```

Pick which slices through the image to back project.

```
        print, '*** SLICE ' + str(slice) + ' ***'
        rbf           = 2                   ; factor by which to reduce
resolution

        filtername = 'RL'           ; name of desired filter: RL or SL

        ; Now read in the corresponding correction data.
        print, 'Reading correction data ...'

        ;dark = read_oct( dark_file )
```

If there is a dark file to correct for then it should be read in here.

```
        ;-------------------------------------------------------------
        ; Read projections from separate files and make sinogram.
        ; This is done for the data set and the correction data set.
        ;-------------------------------------------------------------

        print
        print, 'Reading data...'

        ; Check whether the sinogram exists and, if not, create it.
        result_sino  =  read_idld(  out_dir  +  'data_sino'  +  str(slice)  +
'.idld', /silent )
```

```
        dsz = size(result_sino)

        if ( dsz[0] EQ 0 ) then  begin

            result_sino = fltarr( nx, nproj )
            data_sino = fltarr( nx, nproj )
            left      = indgen(nx/2)
            right     = nx/2+ indgen(nx/2-1)

            for j = 0, nproj-1 do begin

                s = strmid( '0000' + str(j), 3, 4, /reverse_offset )
                proj   =   read_oct(   data_pref   +   s   +   '.oct'   ,
header=hdr_wobble)
                ;proj=proj-dark      ; dark field correction
                data_sino[*,j] = proj[*, slice]

            endfor
            ;stop

            for j = 0, nproj-1 do begin

                ;result_sino[*,j] = alog10(lf_smooth/data_sino[*,j]) ;
                result_sino[*,j]                                          =
alog10(lf_smooth/shift(data_sino[*,j],15.0*sin(j/1000.0*!Pi-0.3*!Pi))) ;
                ;result_sino[*,j] = alog10(1023.0/data_sino[*,j]) ;
            endfor
            write_idld,  out_dir  +  'data_sino'  +  str(slice)  +  '.idld',
result_sino

        endif
        ;stop
        result_sino = shift( result_sino, 0, 0 )
        ;result_sino = shift( result_sino, -10, 0 )
```

The *shift* function can be used to shift the sinogram if the optical axis is off centre, for example if the camera is off centre.

```
        print,   'Time   to   read   data   =',   str(round(systime(1)   -
begin_time)), ' s'
        print, ''

        cal_result_sino = fltarr( nx, nproj )
        cal_result_sino = result_sino
        ;-------------------------------------------
        ; Apply back-projection reconstruction filter
        ; and resize the sinogram if necessary.
        ;-------------------------------------------

        begin_time = systime(1)

        filt_sino     = filter( cal_result_sino, filtername )
        if keyword_set(rbf) then begin
            print, 'Resizing sinogram from ' + str(nx) + ' pixels to ' $
            + str(nx/rbf) + ' pixels...'
            filt_sino     = rebin(filt_sino, nx/rbf, nproj)
            ;filt_sino_mod = rebin(filt_sino_mod, nx/rbf, nproj)
        endif
```

```
        print, 'Time to resize and filter =', str(round(systime(1) -
begin_time)),$
          ' s'
        print, ''

        ;---------------------------------------------------------------
        ; Make initial reconstructed image and then start backprojection
        ;---------------------------------------------------------------

        begin_time = systime(1)

        print, 'Reconstructing with RADON...'

        ; Allow possibility for correction of centre-of-rotation.
        rot_centre_shift = 0

        szl   = size(filt_sino)
        ;theta = findgen( szl[2] ) * 2 * !PI / szl[2]
        theta = findgen( szl[2] ) * !PI / szl[2]
        rho   = (findgen(szl[1]) - szl[1]/2)*rbf + rot_centre_shift

        ; The aim of all the keywords to radon is that the file that
comes out should
        ; be quantitative and representative of the real optical density.
I think
        ; it is now calibrated correctly. When we take a sample
projection from this
        ; dataset, it seems to give approximately the same as log_sino,
which is
        ; what we started with!
        back_projection = radon( transpose(filt_sino), theta=theta,
rho=rho,     $
                        nx=nx/rbf, ny=nx/rbf, dx=rbf, dy=rbf, /backproject
)

        tvscl, back_projection ;< 4

        ;stop

        print, 'Time to backproject =', str(round(systime(1) -
begin_time)), ' s'
        print, ''

        write_idld, out_dir + 'recon' + str(slice) + '.idld',
back_projection

    endfor

end


function filter, data, filtername
; Apply Ram-Lak or Shepp-Logan filter to data.
; Filtername should be either 'RL' or 'SL'.


datasize = size(data)

K = datasize[1]                         ;number of columns in data
if (datasize[0] eq 1) then N = 1                ;number of rows in data
if (datasize[0] eq 2) then N = datasize[2]
```

```
Dxr = 1.0               ;distance between detector elements in number of
pixels
kmax = 1/(2*Dxr)


;----------------
; define filter q
;---------------

if (filtername eq 'SL') then begin                  ;define Shepp-Logan
filter
  i = findgen(2*K-1) - K+1
  q = -8*kmax^2/(!PI^2*(4*i^2-1))
endif

if (filtername eq 'RL') then begin              ;define Ram-Lak filter
  q = fltarr(2*K-1)
  for i = -K+1, K-1 do begin
    if ((i mod 2 eq 0) and (i ne 0)) then q[i+K-1] = 0
    if ((i mod 2 eq 1) or (i mod 2 eq -1)) then q[i+K-1] = (-
4*kmax^2)/(!PI^2*i^2)
    if (i eq 0) then q[i+K-1] = kmax^2
  endfor
endif


;------------------------
; calculate filtered data
;------------------------

filtdata = dblarr(K,N)                                ;initial filtered
data set
for j = 0, N-1 do begin
  ;data[*,j] = data[*,j]/4
  filtdatarowj = convol(q, data[*,j], center=0)
  filtdata[*,j] = filtdatarowj[K-1:2*(K-1)]     ;select right data
endfor

return, filtdata

end
```

The sinogram produced by the IDL program is saved in the form *data_sinoxxx.idld*. This sinogram is processed by a program written in the application Scilab. This application can also be downloaded for free from the internet. To process a sinogram the program `tomoall.sce` is required. The sinogram to be processed should be placed in a separate directory with the program `tomoall.sce`. The program is run by selecting **File** and **Execute** from the Scilab menu. The output file is a two dimensional image of a horizontal slice through the gel. By repeating this for each slice a 3 dimensional reconstruction of the gel is obtained.

Tomoall.sce

```
// Script: Read idld tomography sinogram file and process it.
// Author: Nikola Krstajic
// Date: 20.06.2005
clear
xbasc();
xset("wdim",320,340);
chdir('C:\Documents and Settings\jadp\My Documents\Gels\Reconstruction');
stacksize(12000000);
```

Line 7 in the `tomoall.sce` script must be changed to the new directory containing both the program `tomoall.sce` and the sinogram.

```
// Open the idld file.
[fd,err]=mopen('data_sino40.idld', 'rb');
```

Ensure that the correct sinogram is to be processed is opened here.

```
// Get the character string "SJD ..."
str=mgetstr([15,fd]);

// First byte is before the character string. It should be 1 for windows
operating system.
pos = mseek(0 ,fd, 'set');
plat_win = mget(1,'ucl',fd);

// Number of variables.
pos = mseek(14 ,fd, 'set');
num_vars = mget(1,'ull',fd);

// How many dimensions, usually 2.
pos = mseek(18 ,fd, 'set');
num_dim = mget(1,'ull',fd);

// How many pixels in x?
pos = mseek(22 ,fd, 'set');
x_pixels = mget(1,'ull',fd);

// How many pixels in y?
pos = mseek(26 ,fd, 'set');
y_pixels = mget(1,'ull',fd);

// Start reading the image.
printf("Reading sinogram ...\n")
mat = [];
for i = 1:y_pixels
pos = mseek(38 + x_pixels*4*(i-1) ,fd, 'set');
arr2 = mget(x_pixels,'fl',fd);
mat = [mat; arr2];
end
end_pos = mseek(0 ,fd, 'end');
mclose(fd);
mat = mat';

// Take the logarithm of the whole matrix.
log_mat = -log10(mat);
```

```
printf("Filtering sinogram with Ram Lak.\n")

// Filter data prior to radon transform - Ram-Lak.
kmax = 0.5;
K = x_pixels;
N = y_pixels;
//q = fltarr(2*K-1)
q=zeros(2*K-1);
for i = (-K+1):(K-1)
  //if ((i mod 2 eq 0) and (i ne 0)) then q[i+K-1] = 0
  if modulo(i,2)==0 & i<>0 then
    q(i+K) = 0;
  end
  //if  ((i  mod  2  eq  1)  or  (i  mod  2  eq  -1))  then  q[i+K-1]  =  (-
4*kmax^2)/(!PI*i^2)
  if modulo(i,2)==1 | modulo(i,2)==-1 then
    q(i+K) = (-4*kmax^2)/(%pi*i^2);
  end
  //if (i eq 0) then q[i+K-1] = !PI*kmax^2
  if i==0 then
    q(i+K) = %pi*kmax^2;
  end
end

filtdata = zeros(N,K);
for j = 1:N
  filtdatarowj = convol(q, log_mat(:,j));
  filtdata(j,:) = filtdatarowj(K:(2*K-1));
end

printf("Plotting filtered sinogram.\n")
xset("colormap",graycolormap(1024));
mfiltdata = 1024.0/max(filtdata) .* filtdata;
Matplot(mfiltdata);

filtdata = filtdata';


// This is a SCILAB script that takes filtered back projections without .
// PR is a matrix whose columns are the projections at each angle.

// Determine the size of the projected, PR, image
n = size(filtdata,1);
sideSize = n;

// THETA is a row vector of the angles of the respective projections.
THETA = 0:(180/401):180;

// Convert THETA to radians and subtract pi so the reconstructed image
// has the same orientation
 th = %pi - ((%pi/180)*THETA);

// Prepare image
 m = length(THETA);
 BackI = zeros(sideSize,sideSize);

// Find the middle index of the projections
 midindex = (n+1)/2;

// Create x and y matrices
 x = 1:sideSize;
```

```
 y = 1:sideSize;
 X=[];
 Y=[];

 //[X,Y] = meshgrid(x,y);
 for i=1:768
    X = [X ; x];
 end
 Y=X';

 xpr = X - (sideSize+1)/2;
 ypr = Y - (sideSize+1)/2;

 printf("Backprojecting ...\n")

 for i = 1:m
    // Use the backprojection algorithm to determine which areas on the
projected
    // images add up
    filtIndex = round(midindex + xpr*sin(th(i)) - ypr*cos(th(i)));

    // While "in bounds" then add the point
    BackIa = zeros(sideSize,sideSize);
    spota = find((filtIndex > 0) & (filtIndex <= n));
    newfiltIndex = filtIndex(spota);
    BackIa(spota) = filtdata(newfiltIndex(:),i);

    BackI = BackI + BackIa;
    printf("Projection %i.\n",i)
 end

BackI = BackI./m;

printf("Plotting reconstruction.\n")
xset("colormap",graycolormap(1024));
mBackI = 1024.0/max(BackI) .* BackI;
Matplot(mBackI);
//plot(BackI(350,:))
```